International Journal of Thermofluid Science and Technology (2022)
Volume 9, Issue 1, Paper No. 090102
https://doi.org/10.36963/IJTST.2022090102
Research Article

Effect of some parameters on natural convection heat transfer in finned enclosures- a case study

M. T. Attouchi[1], S. Larbi*, [1] , S. Khelladi[2]

[1]LGMD, Department of Mechanical Engineering, Polytechnic National School of Algiers, 10, Avenue Hassen Badi, El-Harrach, Algiers, Algeria
[2]DynFluid Lab- Arts et Métiers Paris Tech. France.

ARTICLE INFO

Received: 19 July 2021;
Received in revised form:
29 Oct. 2021;
Accepted: 08 Nov. 2021;
Published online:
11 Nov. 2021

Keywords:
Natural Convection
Square cavity
Fined surface
Fluid flow modeling
Numerical simulation

ABSTRACT

In this study, we were interested in free convective heat transfer into cavities with finned surface. The hot horizontal bottom wall with attached fins was under variable (sinusoidal) surface temperature while the cold one, on the upper wall side, was kept at constant temperature. The vertical walls were adiabatic. The developed model is related to laminar natural convection airflow in a finned closed cavity. The considered Rayleigh numbers are in the interval 10^3 to 10^6 while the Prandtl number is 0.7. The finite volume method is used in solving the resulting equations. The developed numerical code is validated owing to benchmark solutions of De Vahl Davis and results reported by other authors. The results presented in this work are linked to the velocity distribution around the surfaces of the fins, the isothermal lines, the streamlines and local and average Nusselt numbers for various geometrical parameters. Special consideration is given to the effects of Rayleigh number, the variable surface hot temperature, the fins number and their length on the fluid flow patterns and heat transfer in square cavities.

1. Introduction

Natural convection problems in cavities with extended surfaces were investigated by many authors. This interest is motivated by various thermal applications such as heating and residential space ventilation, electronic systems cooling and other applications. Nowadays, with the development of efficient algorithms and high speed digital computers, many engineering applications encountered in industry can be solved.

Benard [1] is considered among the pioneer scientists in natural convection research domain. In his experiment, the author observed that the fluid flow motion is in cellular forms. The evaluation of the aspect ratio showed that there was a temperature value below which no convection phenomenon can occur.

The first studies on natural convection in closed cavities were conducted by Batchelor [2]. The cavities may have square or rectangular forms without or with attached fins

*Corresponding e-mail: salah.larbi@g.enp.edu.dz or larbisalah@yahoo.fr (Salah Larbi)

Nomenclature

H	enclosure height, m	x, y	cartesian coordinates
h	fin length, m	x^+, y^+	dimensionless cartesian coordinates
W	enclosure width, m	u, v	velocity components
h	film thickness, m	N	number of fins
w	fin thickness, m	*Greek symbols*	
d	distance between fins, m	ρ	density, kg/m^3
g	gravity, m/s^2	μ	dynamic viscosity, kg/m.s
T	temperature , °C	β	thermal expansion coefficient
p	pressure, Pa	Δ	difference
C_p	specific heat, J/kg.K	*Subscripts*	
Gr	Grashoff number = $\frac{\rho^2 g\beta\Delta T H^3}{\mu^2}$	h	hot
Pr	Prandtl number	c	cold
Ra	Rayleigh number= Gr.Pr	ref	reference
Nu	Nusselt number	w	wall

to one active side. It should be noted that adding fins to cavity surfaces is the most reliable method for increasing the rate of heat transfer in enclosures.

Numerous studies were carried out on free convection in cavities. Bairi et al. [3] summarized some of them. The closed square cavities with simple boundary conditions (adiabatic and uniform temperature profiles) are used as configurations for benchmark testing solutions in the validation of numerical developed programs or CFD packages [4- 6].

Sarris et al. [7] studied numerically the natural free convection in an enclosure where the temperature profile is sinusoidal on the upper wall of the cavity. The Rayleigh numbers used in their study were in the range 10^2 to 10^8. The authors demonstrated that the local Nusselt number at the upper part of the enclosure increased with the increasing of Rayleigh number. Moreover, the fluid flow capacity and thermal penetration depth increased with the increasing of enclosure aspect ratio.

Sathiyamoorthy et al. [8] analyzed the influence of linearly temperature of vertical walls on heat transfer and fluid flow within the square enclosure. The bottom wall is heated uniformly, the top wall is insulated and the left vertical one is considered to be heated in a linear manner while the right vertical wall is either linearly heated or cooled. The Rayleigh and Prandtl numbers used were ($10^3 \leq Ra \leq 10^5$) and ($0.7 \leq Pr \leq 10$) respectively. Galerkin finite element method with penalty parameter is used in solving the resulting partial differential equations. The authors concluded that the numerical method used allows obtaining smooth solutions in terms of stream function and isotherms.

Basak et al. [9] studied the influence of uniform and non- uniform heating cases of the bottom wall in a square cavity on mixed convection. In their physical model, the vertical walls of the enclosure were maintained at a cold and constant temperature while the top wall is insulated. By considering the local Nusselt number evolution, the authors showed that heat transfer rate is important at the edges of the bottom wall and decreased at the center of this wall for the uniform heating case. For the non- uniform heating case of the bottom wall, they noted the opposite; the heat transfer rate is lower at the edges.

Aswatha et al. [10] studied numerically the problem of natural convection in an enclosure. The top wall of the enclosure is adiabatic. The vertical walls are maintained at constant cold temperature. For the horizontal bottom wall, three cases were considered: uniform, sinusoidal and linearly temperature. The Rayleigh numbers considered in their study are in the range 10^3 to 10^7. The Prandtl number related to the working fluid is 0.7 and the aspect ratios are 0.5 and 1. The authors showed that the uniform temperature case

gives high value of Nusselt number compared to sinusoidal and linearly temperature. The average Nusselt number increases with the increase of Rayleigh number for both bottom and side walls.

Ayad et al. [11] analyzed the free convection problem in a cavity with non-uniform hot temperature on the left side wall and cold with uniform temperature on the right side wall of the cavity. The upper and lower walls are considered adiabatic. Governing equations were solved numerically using the finite difference method with a uniform grid size. The effect of Rayleigh number (Ra= 10^3 to 10^5) and enclosure aspect ratio (AR= 1, 3, 5) on flow templates and heat transfer is highlighted. The authors showed that the number of cells vorticity increased with the increasing of the aspect ratio.

Mohapatra et al. [12] analyzed the natural convection in a square cavity where the vertical wall is wavy. The top horizontal wall of the cavity is heated at sinusoidal temperature profile. The three other walls are at uniform cold temperature. The authors illustrated the effect of the corrugated wall on the Nusselt number for different Rayleigh numbers.

About the studies on natural convection in enclosures with attached fins, Yucel and Turkoglo [13] solved numerically the laminar free convection problem in cavities with fins attached to the cold vertical wall. They studied the influence of the fin configuration and the Rayleigh number variation on heat transfer and fluid flow structures. Obtained results showed that heat transfer rate in enclosures with finned surfaces depends essentially on the number of attached fins and their length.

Al-Fahaid [14] analyzed numerically natural convection heat transfer in a vertical finned surface placed on the hot wall of the cavity. The hot as well as the cold vertical walls were kept at constant temperatures. The study showed that the rate of heat transfer through the cavity is influenced by the number of the attached fines, the Rayleigh number and their lengths. Since then, numerous studies on natural convection in finned surfaces have been carried out, both experimentally and theoretically [15- 22]. Among the important recent theoretical studies conducted on optimization of fins in confined cavities we cite the study presented by Azimifar and Payan [23]. The authors used PSO algorithm for obtaining optimal characteristics of an array of fins in an enclosure. References [24- 29] report recent theoretical works in enclosures with finned surfaces under free convection.

As far as we know, based on the literature review, no comprehensive study was reported on natural convection in cavities with finned surfaces where one surface is kept at periodic wall temperature.

In this study, laminar natural convection heat transfer in a square cavity with conducting fins is analyzed. The fins are attached to the hot horizontal bottom side which is at variable (sinusoidal) surface temperature. The cold horizontal top side is at constant temperature while the vertical walls are kept adiabatic. The considered Rayleigh numbers are in the range 10^3 to 10^6 while the Prandtl number is 0.7. Fluid dynamics and thermal aspects of the airflow were deeply analysed owing to the numerical solutions of the resulting equations. The present work is specifically focused on the effects of variable surface hot temperature, the Rayleigh number, the fins number, their spacing and length on fluid flow patterns and heat transfer.

2. Methodology

Fig. 1 illustrates the geometry of the studied model. It is related to an enclosure with seven fins attached to the horizontal bottom wall.

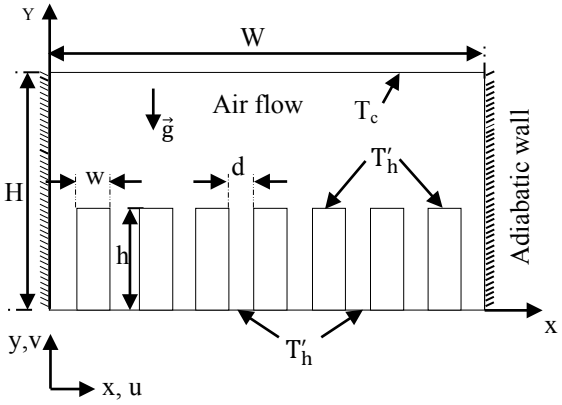

Fig.1. Physical model used.

The considered problem is two-dimensional and the fluid flow is laminar natural convection in a cavity. The horizontal top wall of the enclosure is maintained at cold temperature, T_c, The bottom wall is at sinusoidal hot temperature profile, T'_h while the vertical walls are maintained adiabatically.

2.1 Resulting equations

The following equations are based on conservative equations which are:

$$\frac{\partial \rho}{\partial t} + \frac{\partial (\rho u)}{\partial x} + \frac{\partial (\rho v)}{\partial y} = 0 \tag{1}$$

For continuity equation

$$\rho \frac{\partial u}{\partial t} + \rho u \frac{\partial u}{\partial x} + \rho v \frac{\partial u}{\partial y} = -\frac{\partial p}{\partial x} + \frac{\partial}{\partial x}\left(2\mu \frac{\partial u}{\partial x}\right) + \frac{\partial}{\partial y}\left(\mu\left(\frac{\partial u}{\partial y} + \frac{\partial v}{\partial x}\right)\right) \tag{2}$$

For momentum equation corresponding to x abscise

$$\rho\frac{\partial v}{\partial t} + \rho u\frac{\partial v}{\partial x} + \rho v\frac{\partial v}{\partial y} = -\frac{\partial p}{\partial y} + \frac{\partial}{\partial y}\left(2\mu\frac{\partial v}{\partial y}\right) + \frac{\partial}{\partial x}\left(\mu\left(\frac{\partial u}{\partial y} + \frac{\partial v}{\partial x}\right)\right) + \rho g\beta\left(T - T_{ref}\right) \tag{3}$$

For momentum equation corresponding to y component, and

$$\rho\frac{\partial T}{\partial t} + \rho u\frac{\partial T}{\partial x} + \rho v\frac{\partial T}{\partial y} = \frac{\partial}{\partial x}\left(\frac{\mu}{\mathrm{Pr}}.\frac{\partial T}{\partial x}\right) + \frac{\partial}{\partial y}\left(\frac{\mu}{\mathrm{Pr}}\frac{\partial T}{\partial y}\right) \tag{4}$$

For energy equation.

The buoyancy term, due to the variation of density, is obtained also by using the Boussinesq's approximation.

The previous equations of equilibrium (1- 4) can be expressed as follows:

$$\frac{\partial}{\partial t}(\rho\phi) + \frac{\partial}{\partial x}(\rho u\phi) + \frac{\partial}{\partial y}(\rho v\phi) = \frac{\partial}{\partial x}\left(\Gamma^{\phi}\frac{\partial \phi}{\partial x}\right) + \frac{\partial}{\partial y}\left(\Gamma^{\phi}\frac{\partial \phi}{\partial y}\right) + S^{\phi} \tag{5}$$

The assumptions used in this study correspond to Newtonian, incompressible fluid, with non- viscous dissipation and without heat source.

At steady state and in dimensionless form, equation 5 can be written as:

$$\frac{\partial}{\partial x^+}\left(u^+\phi^+\right) + \frac{\partial}{\partial y^+}\left(v^+\phi^+\right) = \frac{\partial}{\partial x^+}\left(\Gamma^{\phi^+}\frac{\partial \phi^+}{\partial x^+}\right) + \frac{\partial}{\partial y^+}\left(\Gamma^{\phi^+}\frac{\partial \phi^+}{\partial y^+}\right) + S^{\phi^+} \tag{6}$$

Where

$$x^+ = \frac{x}{W},\ y^+ = \frac{y}{H},\ u^+ = \frac{u}{u_{ref}}, v^+ = \frac{v}{u_{ref}}, T^+ = \frac{T - T_{ref}}{\Delta T}, \tag{7}$$
$$p^+ = \frac{p}{p_{ref}}, u_{ref} = \sqrt{g\beta H\Delta T}, T_{ref} = \frac{(T_c + T_h)}{2}, p_{ref} = \rho u_{ref}^2$$

Such as:$\Delta T = T_h - T_c$.T_h and T_c are respectively the hot and the cold temperatures.

The dimensionless variables become then

$$u^+ = \frac{u\rho H}{\mu Gr^{0.5}},\ v^+ = \frac{v\rho H}{\mu Gr^{0.5}},$$
$$p^+ = \frac{\rho p H^2}{\mu^2 Gr},\ Gr = \frac{\rho^2 g\beta\Delta T H^3}{\mu^2}, \tag{8}$$
$$\mathrm{Pr} = \frac{\mu c_p}{k}, Ra = \frac{\rho^2 g\beta\Delta T H^3 \mathrm{Pr}}{\mu^2}$$

The following Table 1 gives the correspondence between ϕ^+, $\Gamma^{\phi^+}, S\phi^+$and the balance equations.

Table 1

Correspondence between the symbols, ϕ^+, $\Gamma^{\phi^+}, S\phi^+$ and the balance equations.

Equation	ϕ^+	Γ^{ϕ^+}	$S\phi^+$
of Continuity	1	0	0
of Momentum vs. x component	u^+	$\sqrt{\frac{Pr}{Ra}}$	$-\frac{\partial p^+}{\partial x^+} - \frac{2u^+}{x^{+2}}\sqrt{\frac{Pr}{Ra}}$
of Momentum vs. y component	v^+	$\sqrt{\frac{Pr}{Ra}}$	$-\frac{\partial p^+}{\partial y^+} + T^+$
of Energy	T^+	$\frac{1}{\sqrt{Pr.Ra}}$	0

The local Nusselt numbers along the lower part and the upper part of the horizontal cavity wall are defined respectively by

$$\mathrm{Nu_{Lower}} = -\left.\frac{\partial \mathrm{T}^+}{\partial \mathrm{y}^+}\right|_{\mathrm{y}^+=0} \tag{9}$$

$$\mathrm{Nu_{Upper}} = -\left.\frac{\partial \mathrm{T}^+}{\partial \mathrm{y}^+}\right|_{\mathrm{y}^+=1} \tag{10}$$

The average Nusselt can be deduced by integrating the local Nusselt number along the cavity wall. Then

$$\overline{Nu} = \int_0^1 - \frac{\partial T^+}{\partial y^+} dx^+ \quad (11)$$

2.2. Boundary conditions

The no-slip and Neumann or Dirichlet conditions are used as boundary conditions for velocity and temperature respectively. The fins are considered heated at variable temperature with a sinusoidal form, T_h', given by:

$$T_h' = (T_h - T_c) sin\left(\frac{\pi x}{W}\right) + T_c$$

In dimensionless form, the boundary conditions related to the temperature are:

$T^*(x^+,0) = sin(\pi x^+)$: Sinusoidal temperature profile at the horizontal bottom wall of the enclosure and the entire finned surface.

$$- \frac{\partial T^+}{\partial y^+}\left(x^+,1\right) = 0 \quad \text{and} \quad T^+\left(0,y^+\right) = T^+\left(1,y^+\right) = 0$$

The boundary conditions related to the dimensionless velocity are:

- $u^+(x^+, 0) = 0$; $u^+(0, y^+) = 0$; $u^+(1, y^+) = 0$.

- $u^+(x^+, 1) = 0$ at the fins surface.

3. Numerical resolution and validation

The two-dimensional general discretized equation of space can be presented as:

$$a_P\phi_P = a_E\phi_E + a_W\phi_W + a_N\phi_N + a_S\phi_S + S \quad (12)$$

Where a_P, a_E, a_W, a_N and a_S are the coefficients related to the variable φ.

The initial and final two-dimensional discretized form can be written as:

$$\frac{(\rho_P u_P - \rho_P^0 u_P^0)\Delta x\Delta y}{\Delta t} + J_e - J_w + J_n - J_s = (S_C + S_P u_P)\Delta x\Delta y \quad (13)$$

Where:

$$J_e = \left\{(\rho u)_e u - (\mu + \mu_t)_e \frac{\partial u}{\partial x}\right\}\Delta y$$

$$J_w = \left\{(\rho u)_w u - (\mu + \mu_t)_w \frac{\partial u}{\partial x}\right\}\Delta y$$

$$J_n = \left\{(\rho v)_n u - (\mu + \mu_t)_n \frac{\partial u}{\partial y}\right\}\Delta x$$

$$J_s = \left\{(\rho v)_s u - (\mu + \mu_t)_s \frac{\partial u}{\partial y}\right\}\Delta x$$

$S = S_C + S_P u_P$: represents the source term.

The final discretized form is

$$a_P u_P = a_E u_E + a_W u_W + a_N u_N + u_S \phi_S \quad (14)$$

Where:

$a_E = D_e A(|P_e|) + [\![- F_e, 0]\!]$

$a_W = D_w A(|P_w|) + [\![- F_w, 0]\!]$

$a_N = D_n A(|P_n|) + [\![- F_n, 0]\!]$

$a_S = D_S A(|P_s|) + [\![- F_s, 0]\!]$

The symbol [[]] represents the largest part of the quantity contained within it. Then:

$$a_P^0 = \frac{\rho_P^0 \Delta x \Delta y}{\Delta t}$$

$$S = S_C \Delta x \Delta y + a_P^0 u_P^0 + M$$

$$a_P = a_E + a_W + a_N + a_S + a_P^0 - S_P \Delta x \Delta y \quad (15)$$

Where:

$$F_e = (\rho u)_e \Delta y \; ; D_e = \frac{(\mu + \mu_t)_e \Delta y}{(\delta x)_e} \; ; P_e = \frac{F_e}{D_e} ;$$

$$F_w = (\rho u)_w \Delta y \; ; D_w = \frac{(\mu + \mu_t)_w \Delta y}{(\delta x)_w} \; ; P_w = \frac{F_w}{D_w}$$

$$F_n = (\rho v)_n \Delta x \; ; D_n = \frac{(\mu + \mu_t)_n \Delta x}{(\delta y)_n} \; ; P_n = \frac{F_n}{D_n} ;$$

$$F_s = (\rho v)_s \Delta x \; ; D_s = \frac{(\mu + \mu_t)_s \Delta x}{(\delta y)_s} \; ; P_s = \frac{F_s}{D_s}$$

F, represent*s* the mass flow rates through the faces of the control volume or the strength of convection. P, the Peclet number which is the ratio of the strengths of convection and diffusion. *D* ,the strength of diffusion.

The subscripts in lower case represent values at the faces of the control volume. *A* ($|P|$) represents the function that provides the expressions of the different discretization schemes.

A relationship between the pressure and the velocity is deduced. It is used in the continuity equation in order to derive the equation of pressure correction. Referring to Patankar [30], a detailed derivation of the pressure correction equation is discussed where the main principal steps of the derivation are given.

Let p the corrected pressure, p* the guessed pressure and p' the pressure correction where:

$$p = p^* + p' \quad (16)$$

An analogous equation can be deduced for the corrected velocities, *u* and *v*:

$$u = u^* + u' \; ; \; v = v^* + v' \quad (17)$$

Where $u'$and $v'$are the velocity corrections, and $u^*$and $v^*$are the guess velocities.

The velocity correction formulas are defined as:

$$u' = d_w(p_w - p'_P);\ v' = d_s(p'_S - p) \qquad (18)$$

Where:

$$d_w = \frac{A_{ew}}{a_P} \quad \text{and} \quad d_s = \frac{A_{ns}}{a_P}$$

A_{ew} and A_{ns} represent areas associated with the East-West and North-South directions respectively.

Equation (18) gives a relationship between the pressure correction and the velocity correction. Then, we can now write equation (17) as:

$$u = u^* + d_w(p'_W - p'_P)$$
$$v = v^* + d_s(p'_S - p) \qquad (19)$$

The resulting equations are used in their dimensionless form in the numerical simulation to reduce the number of independent parameters. In addition, they offer them more general solution by reducing the machine computational time and by increasing the solution of the convergence speed.

Prandtl and Rayleigh are the dimensionless numbers used in these equations. Numerical modeling of the problem is achieved starting from the resolution of the fluid dynamics equations using the finite volume method with appropriate boundary conditions [30- 32]. The Rayleigh numbers used are in the range 10^3 to 10^6 while the Prandtl number is 0.71.

The mesh grids used in the calculation code are of different sizes according to the geometry of the cavity, the required precision and the geometry considered near or at a distance from the walls. The cell size ranges from 102 × 102 to 402 × 402. Convergence criteria is ensured by a stop test of 10^{-6} and applied in the calculation code based on the residuals of T, u and v.

In all calculations, under-relaxation factors with values of 0.4, 0.4, 0.8, and 0.5 were applied to u, v, T, and p, respectively.

3.1. Grid independence test analysis

A grid independence test study is conducted using different grid sizes, 20x20, 40x40 60x60, 80x80, 100x100 and 200x200 for different Rayleigh numbers (10^3, 10^4, 10^5 and 10^6).

Figs 2 and 3 illustrate the evolution of the average Nusselt number $\overline{Nu}$ versus the grid size for three Rayleigh numbers (10^4, 10^5 and 10^6) and for bottom and top wall sides of the enclosure respectively. Notice that the average Nusselt number increases with the increase of the Rayleigh numbers and all the curves are stabilized beyond a certain grid size value.

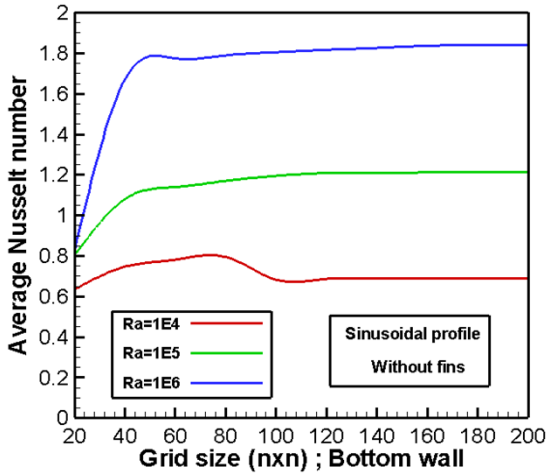

Fig. 2 Evolution of the average Nusselt number $\overline{Nu}$ on the bottom wall side of the enclosure versus the grid size for different Rayleigh numbers.

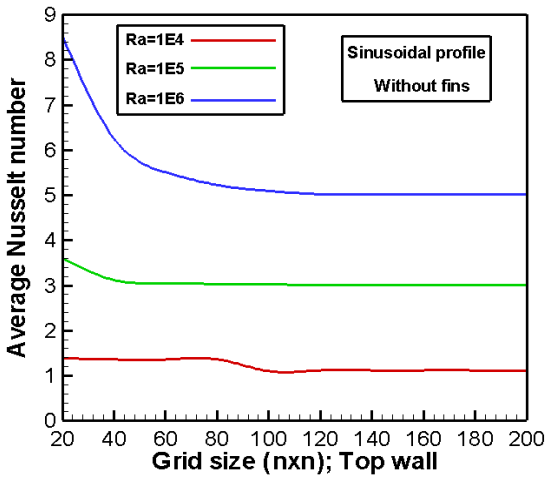

Fig. 3 Evolution of the average Nusselt number $\overline{Nu}$ on the top wall side of the enclosure versus the grid size for different Rayleigh numbers.

3.2. Code validation

The numerical code developed in this study is in FORTRAN language. It was validated by the Benchmark testing solutions relating to the problem of free convection in enclosure. The code validation was also carried

out by comparison with other results from the literature review.

Table 2 illustrates the good agreement of maximum, minimum and average Nusselt numbers between the present study and the numerical results presented in the literature review: Barakos et al. [5], Wan et al. [4] and De Vahl Davis [6].

Table 2
Minimum, average and maximum Nusselt numbers results. Comparison between the present study and others.

Ra	Nu	Wan et al.[4]	Barakos et al. [5]	De Vahl Davis[6]	Present study
10^3	Max	1.501- 1.444	1.50	1.47	1.506
	Min	0.691- 0.665	0.692	0.623	0.697
	Average	1.117- 1.073	1.12	1.074	1.1008
10^4	Max	3.576- 3.441	3.53	3.47	3.535
	Min	0.577- 0.5 28	0.586	0.497	0.605
	Average	2.25 - 2.155	2.243	2.084	2.225
10^5	Max	7.945 - 7.662	7.71	7.71	7.724
	Min	0.698- 0.678	0.729	0.614	0.784
	Average		4.52	4.3	4.486
10^6	Max	17.86- 17.39	17.92	17.46	17.4912
	Min	0.9132- 0.903	0.989	0.716	1.185
	Average	8.976 - 8.632	8.8	8.743	8.7268

4. Results and discussion

The results are related to local and average Nusselt numbers, the isotherms, the streamlines and the iso-velocity components distributions around the finned surface of the enclosure versus the fins number and some geometrical parameters.

4.1. Results comparison

Figs. 4 and 5 illustrate the results comparison between the present work and Al-Amiri et al. [17] for two Rayleigh numbers (10^4 and 10^5) with Pr =0.71.These results are related to the streamlines and isotherms contours versus Rayleigh numbers for one fin. Notice the good agreement between the results obtained in this study and those reported by Al- Amiri et al. [17].

To validate the obtained results, a comparison with experimental data is done. The experimental device used is a 2D PIV apparatus. Fig. 6 illustrates the streamline results comparison, for one fin, between this study and experimental measurements of Corvaro and Paronchini [33] for two Rayleigh numbers, Ra = $6.39.10^4$ and Ra=$3.16.10^5$ with Pr=0.71. Good agreement is noted between our results and experimental measurements.

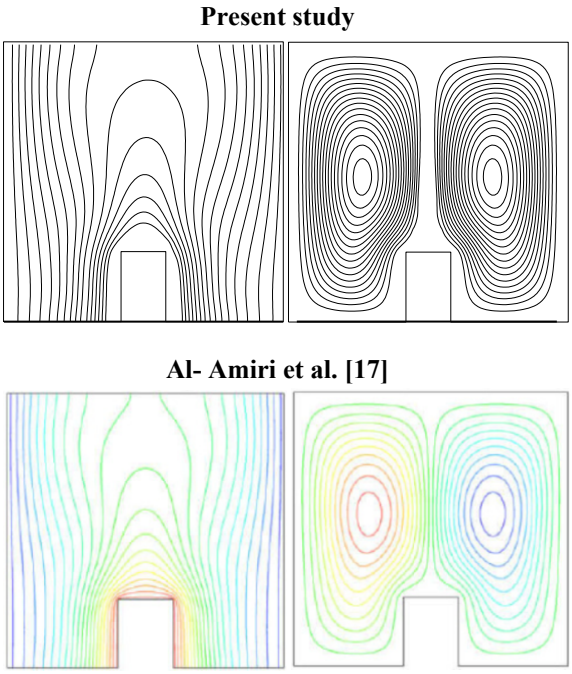

Fig. 4 Isothermal and stream lines for: Ra=10^4, Pr=0.71. Results comparison between the present study and Al- Amiri et al. [17] results.

Present study

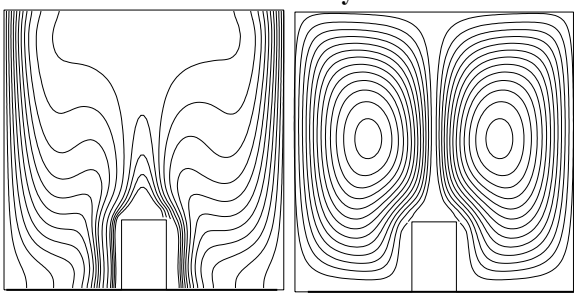

Al- Amiri et al. [17]

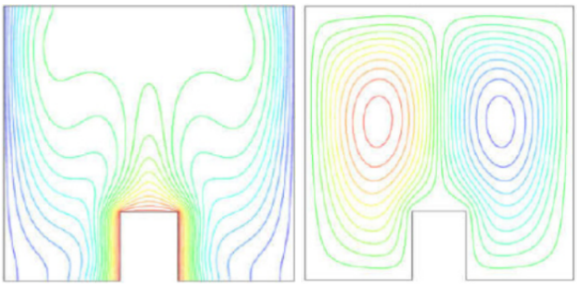

Fig. 5 Isothermal and stream lines for: Ra=10^5, Pr=0.71. Results comparison between the present study and Al- Amiri et al. [17] results.

Present study

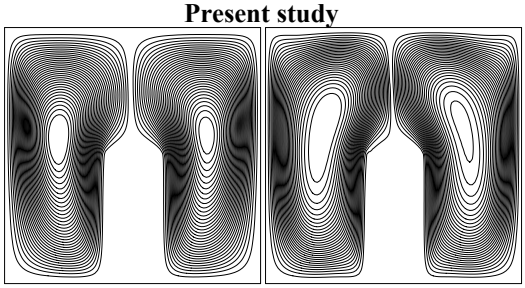

Corvaro and Paroncini [33]

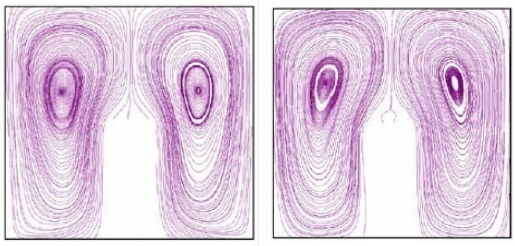

Fig. 6 Stream lines for: Ra = 6.39.10^4 (Left), Ra=3.16.10^5(Right) with Pr =0.71. Results comparison.

4.2. Effect of the sinusoidal temperature profile

The effect of the variable hot temperature profile on heat transfer rate and circulation patterns in the enclosure is depicted in Figs 7 - 14. Notice that the considered enclosure is without any fin or array of fins.

Figs 7- 10 illustrate the isotherms, the streamlines and the iso-velocity contours (u and v) for two Rayleigh numbers (10^3 and 10^6) respectively. For the weak Rayleigh numbers, the isothermal lines are mostly horizontal and parallel to each other which characterize the conductive heat transfer.

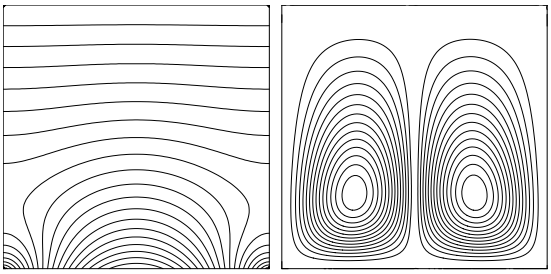

Fig. 7. Isothermal and stream lines for: Ra=10^3 and Pr=0.71.

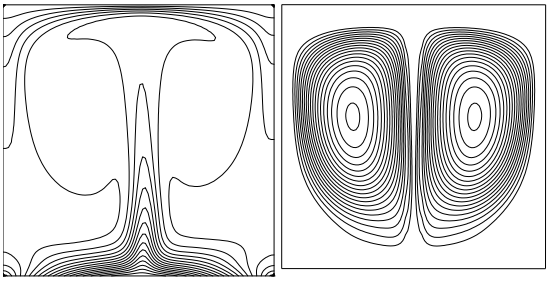

Fig. 8 Isothermal and stream lines for: Ra=10^6 and Pr=0.71.

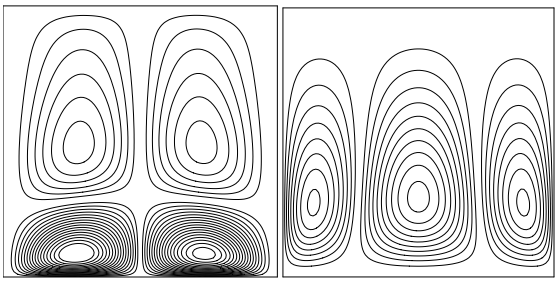

Fig. 9 Iso-velocity contours (u and v) for: Ra=10^3 and Pr=0.71.

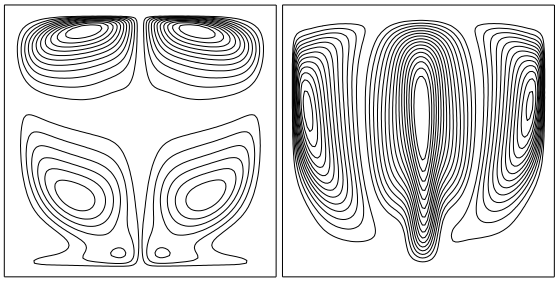

Fig. 10 Iso-velocity contours (u and v) for: Ra=10^6 and Pr=0.71.

Near the hot wall, the isothermal lines are not parallel owing to the sinusoidal temperature profile at the hot wall of the enclosure. With increasing the Rayleigh numbers, up to 10^4, the buoyancy driven forces will be important and natural convection will be the dominant mode of heat transfer.

The isotherms are then mostly non parallel to the horizontal cold wall. Notice that according to the symmetry of the boundary conditions used, the fluid flow and temperature distributions are also symmetric compared to the x- mid-plane of the enclosure.

The streamlines are characterized by two counter- rotating cells and these cells are symmetrically deformed according to the fluid flow which moves from the hot to the cold wall.

The iso-velocity contours related to u-component are characterized by the presence of four cells. The two upper cells are very tight against the cold part of the enclosure following to the direction of the fluid movement. Those of v-component are described by three cells. The size of the central cell is much important than the two others according to the temperature profile of the hot wall of the enclosure.

The evolution of the local Nusselt number versus X abscise at the cold and hot walls are depicted in Figs. 11- 14 where we note the effect of the Rayleigh number and the sinusoidal temperature profile on the local Nusselt number.

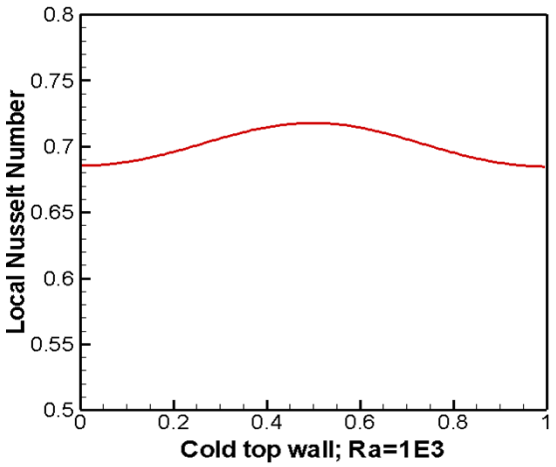

Fig. 11 Evolution of the local Nusselt number on the cold wall versus X abscise for: Ra=10^3 and Pr=0.71.

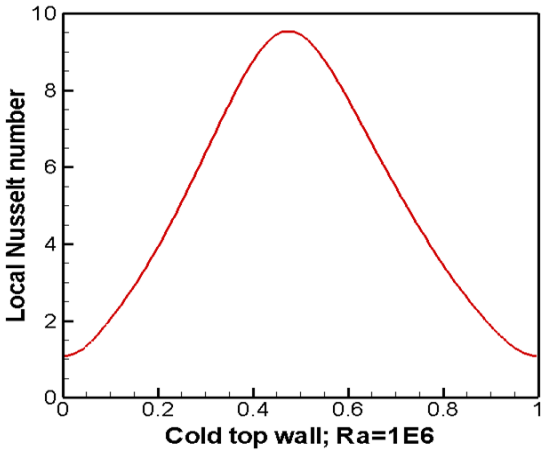

Fig. 12 Evolution of the local Nusselt number on the cold wall versus X abscise for: Ra=10^6 and Pr=0.71.

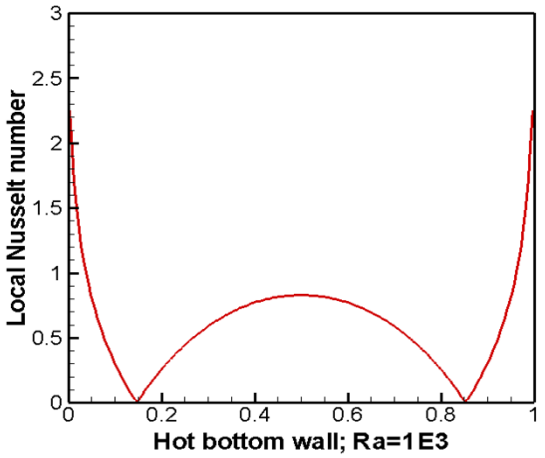

Fig. 13 Evolution of the local Nusselt number on the hot wall versus X abscise for: Ra=10^3 and Pr=0.71.

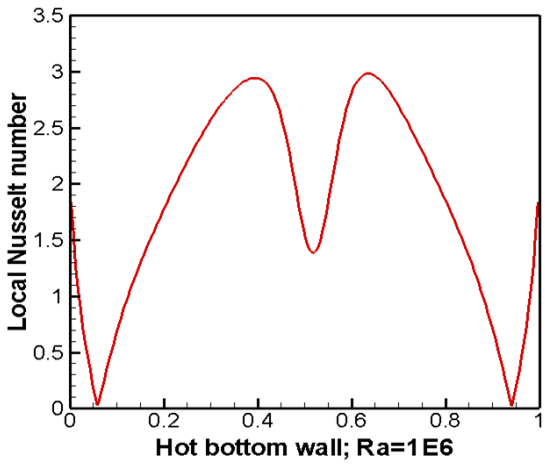

Fig. 14 Evolution of the local Nusselt number on the hot wall versus X abscise for: Ra=10^6 and Pr=0.71.

The velocity v- component distributions at the horizontal mid- section of the enclosure versus X coordinate, for different Rayleigh number values, are plotted in Fig. 15. For the weak Rayleigh number values, the fluid flow velocity is zero which corresponds to the conductive heat transfer mode as described previously.

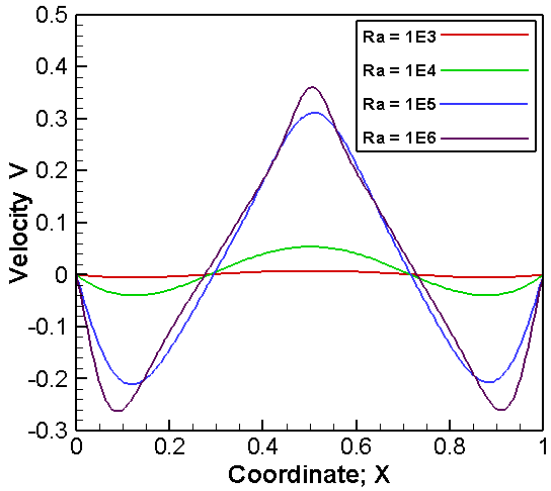

Fig. 15 Evolution of the velocity, V component, at the horizontal mid-section of the enclosure versus X coordinate for different Rayleigh number values.

4.3. Effect of the fin numbers

Fig. 16 shows the isotherms, the streamlines and the iso-velocity (u and v) contours for different fin numbers (N=1, 3, 7) with h/H=0.20, w/W=0.05 and for: $Ra=10^3$. The symmetrical behavior of the flow templates is illustrated in all these figures.

The isothermal lines are mostly parallel to the cold side of the enclosure for all the fin number cases which characterize the conductive heat transfer phenomenon. Closely to the horizontal hot side, the isotherms are not parallel according to the sinusoidal temperature profile on the boundary condition used at the horizontal bottom side of the enclosure.

By increasing the Rayleigh number, this parallelism disappears in approximately all the cavity. Natural convection will then be the dominant heat transfer mode, except along the top cold side where some isothermal lines remain parallel due to the development of a thin thermal boundary layer at this side. A plume- like form of the fluid flow appears at the mid-plane of the hot side of the enclosure and this form is extended (Fig. 17).

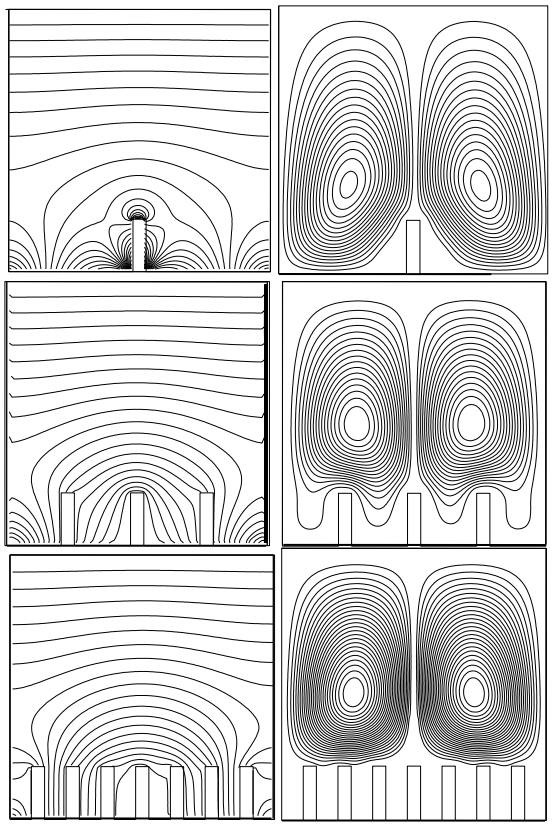

Fig. 16 Isothermal and stream lines for different number of fins with h/H=0.20, w/W=0.05 and for: $Ra=10^3$ and Pr=0.71.

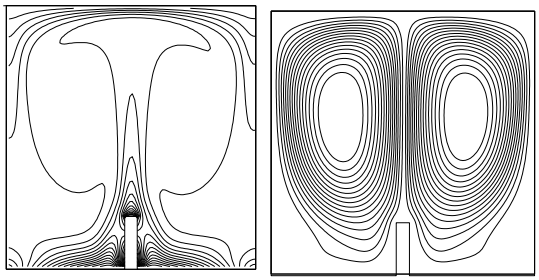

Fig. 17 Isothermal and stream lines for one fin with h/H=0.20, w/W=0.05 and for: $Ra=10^6$ and Pr=0.71.

4.4. Effect of the Rayleigh number

The average Nusselt number evolution versus the Rayleigh number for different fin numbers (N= 0 to 7) with h/H=0.20 and w/W=0.05 at the hot and cold sidewalls of the cavity is plotted in Figs 18 and 19 respectively.

As depicted in these figures, the Nusselt number increases with the increase of the Rayleigh number for fins number ranging from

0 to 7 fins. The maximum value of the Nusselt number is reached at Ra= 10^6 and this value is depending on the fin number.

Fig.18 illustrates that at Ra= 10^6, the Nusselt number is in the range 2 to 21 while Fig. 19 shows the Nusselt number in the range 5 to 7.25. Notice that the maximum value of average Nusselt number is reached for three fins case near the hot side of the cavity.

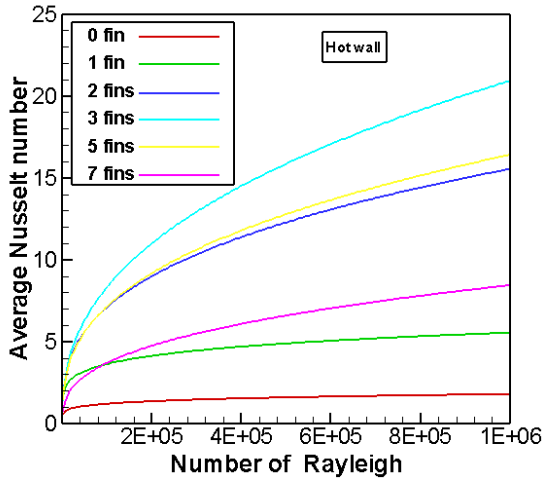

Fig. 18 Evolution of the average Nusselt number at the hot wall versus Rayleigh number for different numbers of fin (N=0 to 7) with: h/H=0.20 and w/W=0.05.

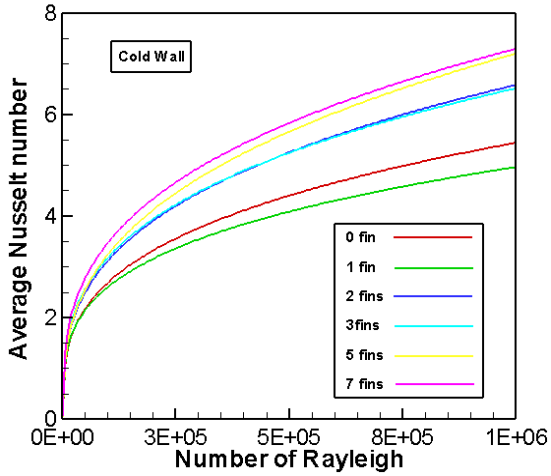

Fig. 19 Evolution of the average Nusselt number at the cold wall versus Rayleigh number for different numbers of fin (N= 0 to 7) with: h/H=0.20 and w/W=0.05.

The average Nusselt number evolution versus fin numbers for different Rayleigh numbers with h/H=0.20 and w/W=0.05 at hot and cold side walls of the enclosure is displayed in Figs. 20 and 21 respectively.

The maximum of Nusselt number value is reached for the case of enclosure with three fins at the hot sidewall. At the cold sidewall, the Nusselt number is approximately constant regardless of the fins number for Ra= 10^3, 10^4 and 10^5. For Ra= 10^6, the Nusselt number increases with the increase of Rayleigh number. It is approximately constant for fin numbers between 2 and 5 fins.

Then, near the cold side, the average Nusselt number is closely affected by the fins number.

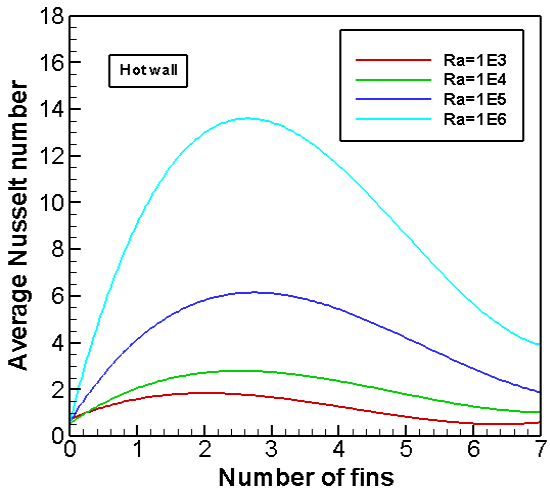

Fig. 20 Evolution of the average Nusselt number at the hot wall versus fin numbers for different Rayleigh numbers with: h/H=0.20 and w/W=0.05.

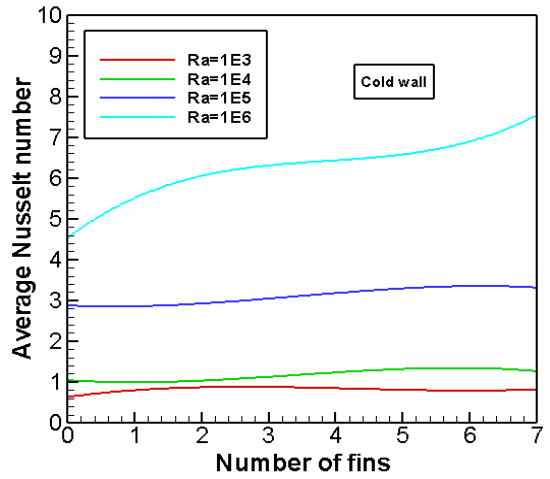

Fig. 21 Evolution of the average Nusselt number at the cold wall versus fin numbers for different Rayleigh numbers with: h/H=0.20 and w/W=0.05.

4.5. Effect of the fin length

Figs. 22 and 23 show the evolution of average Nusselt number versus fin numbers for different values of fin length and for Ra= 10^4 at the hot and cold sidewalls of the enclosure respectively.

At the hot sidewall, the maximum value of average Nusselt number is reached for enclosure of three fins case as specified previously with fin length equals to 0.6.

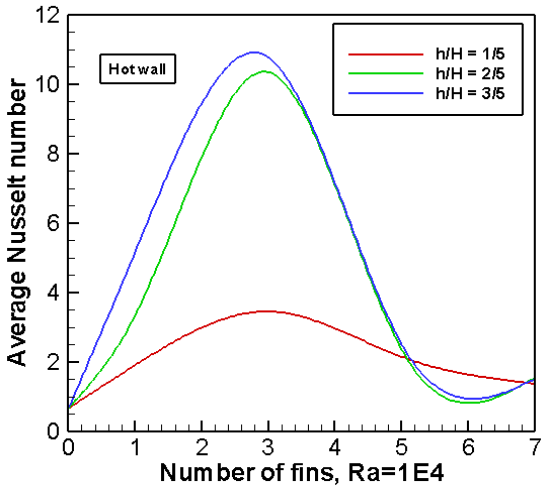

Fig. 22 Evolution of the average Nusselt number at the hot wall versus fin numbers for different values of h/W and for Ra= 10^4.

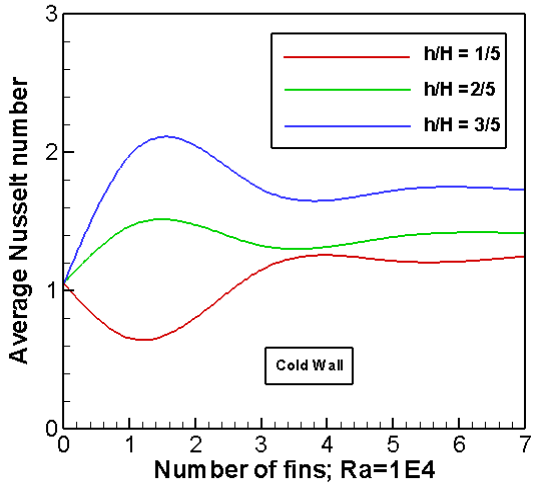

Fig. 23 Evolution of the average Nusselt number at the cold wall versus fin numbers for different values of h/W and for Ra= 10^4.

The minimum value of average Nusselt number is obtained for the case of six fins with the same value of fin length i.e 0.6. At the cold sidewall, up to three fins, the average Nusselt number is approximately constant for each value of fin length.

The evolution of the average Nusselt number versus fin numbers for different values of fin length and for Ra= 10^6 at hot and cold sidewalls of the enclosure is displayed in Figs. 24 and 25 respectively.

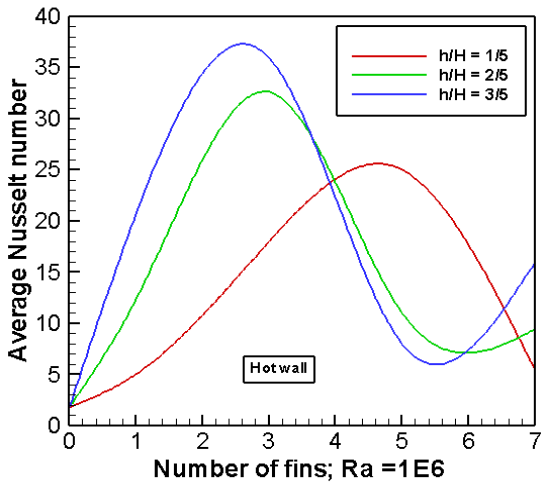

Fig. 24 Evolution of the average Nusselt number at the hot wall versus fin numbers for different values of h/W and for Ra= 10^6.

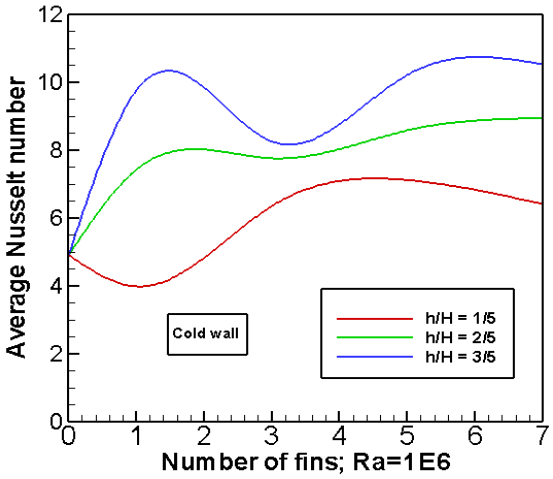

Fig. 25 Evolution of the average Nusselt number at the cold wall versus fin numbers for different values of h/W and for Ra= 10^6.

By increasing the Rayleigh number from its previous value 10^4 to 10^6, the average Nusselt number increases from 11 to 37 at the hot sidewall and from 1.6 to 8 at the cold sidewall. The increase in Rayleigh number induces the enhancement of heat transfer. The

same observations about the maximum and minimum values of average Nusselt number remain also valuable for these last figures.

5. Conclusions

This work is devoted to natural convection heat transfer in a square cavity with finned surface where one surface is kept at periodic wall temperature.

The finite volume method is used to solve the fluid dynamics equations with the appropriate boundary conditions. Four Rayleigh numbers ranging from 10^3 to 10^6 and a Prandtl number of 0.71 are considered.

The developed numerical code is firstly validated owing to the benchmark solutions of natural convection in a square closed cavity for different Rayleigh numbers and secondary by comparison with the results reported by others from the literature review.

The presented results are linked to isothermal lines, streamlines, airflow velocities and Nusselt number for different geometrical parameters. The current study is specifically focused on the effects of the Rayleigh number, the variable surface hot temperature, the fins number, their spacing and their length on the fluid flow templates and heat transfer in square enclosures.

Obtained results showed:

1) - The Nusselt number increases with the increase of Rayleigh number.

2) - For the weak Rayleigh numbers, the isotherms are mostly horizontal and parallel to each other which characterize the conductive heat transfer.

3) - With increasing Rayleigh number, up to 10^4, the buoyancy driven forces will be important and natural convection will be the dominant mode of heat transfer.

4) - According to the symmetry of the boundary conditions used, the fluid flow and temperature distributions are symmetric compared to the x- midplane of the enclosure.

5) - The maximum value of average Nusselt number is reached for the case of enclosure with three fins at the hot sidewall.

6) - At the cold sidewall, the average Nusselt number is approximately constant regardless of the fin numbers for Ra= 10^3, 10^4 and 10^5.

7) -The obtained results are in good agreement with those reported in the literature.

References

[1] T. Benard, Les tourbillons cellulaires dans une nappe liquide, Rev. Gen. Sci., Pure Appl. 11 (1900) 1309–1328.

[2] G. K Batchelor, Heat transfer by free convection across a closed cavity between vertical boundaries at different temperatures, Appl. Math. 12 (1954) 209–230.

[3] A. E. Bairi, E. Zarco-Pernia, G. M. García de María, A review on natural convection in enclosures for engineering applications. The particular case of the parallelogrammic diode cavity, App. Therm. Eng. 63 (2014) 304-322.

[4] D. C. Wan, B. S. V. Patnaik, G. W. Wei, A new benchmark quality solution for the buoyancy-driven cavity by discrete singular convolution, Num. Heat Trans. 40 (2010) 199-228.

[5] G. Barakos, E. Mitsoulis, D. Assimacopoulos, Natural convection flow in a square cavity revisited: Laminar and turbulent models with wall functions, Int. J. Num. Meth. Flui. 18 (1994) 695-719.

[6] D. De Vahl Davis, Natural convection of air in a square cavity : a benchmark solution, Int. J. Numer. Meth. Flui. 3 (1983) 249-264.

[7] I. E. Sarris, I. Lekakis, N. S. Vlachos, Natural convection in a 2d enclosure with sinusoidal upper wall temperature, Num. Heat Trans., Part A. 42 (2002) 513- 530.

[8] M. Sathiyamoorthy, T. Basak, S Roy, I. Pop, Steady natural convection flows in a square cavity with linearly heated side wall(s), Int. J. Heat Mass Trans. 50 (2007)766–775.

[9] T. Basak, S. Roy, P. K. Sharma, I. Pop, Analysis of mixed convection flows within a square cavity with uniform and non-uniform heating of bottom wall, Int. J. Ther. Sci. 48 (2009) 891–912.

[10] C. J. Aswatha1, G. Gowda, S. N. Sridhara, K. Seetharamu, Buoyancy driven heat transfer in cavities subjected to thermal boundary conditions at bottom wall, J. Appl. Fluid. Mech. 5 (2012) 43–53.

[11] M. S Ayad, S. A. Israa, A. H. Saib, Natural convection heat transfer in rectangular enclosure with sinusoidal boundary condition, J. Eng. Dev. 16 (2012) 287–306.

[12] R. C. Mohapatra, Study on natural convection in a square cavity with wavy right vertical wall filled with viscous fluid, J. Mech. and Civil Eng. 14 (2017) 32–39.

[13] N. Yucel, H. Turkodlo, Numerical analysis of laminar natural convection in enclosures with fins attached to an active wall, Int. J. Heat Mass Trans. 33 (1998) 307- 314.

[14] A. F. Al-Fahaid, Numerical study of conjugate heat transfer in enclosures with fins attached to a vertical side wall, Kuwait J. Sci. Eng. 33 (2006) 205- 218.

[15] H. Oztop, E. Bilgem, Natural convection in differentially heated and partially divided square cavities with internal heat generation, Int. J. Heat Fluid Flow. 27 (2006) 466–475.

[16] S. K. Mahapatra, A. Sarkar, Numerical simulation of opposing mixed convection in differentially heated square enclosure with partition, Int. J. Ther. Sci. 46 (2007) 970–979.

[17] A. Al Amiri, K. Khanafer, I. Pop, Buoyancy-induced flow and heat transfer in a partially divided square enclosure, Int. J. Heat Mass Trans. 52 (2009) 3818–3828.

[18] V. Geniy, K Mikhail, A Sheremet, Numerical simulation of turbulent natural convection in a rectangular enclosure having finite thickness walls, Int. J. Heat Mass Trans. 53 (2010) 163–177.

[19] V. A. F. Costa, Natural convection in partially divided square enclosures: Effects of thermal boundary conditions and thermal conductivity of the partitions, Int. J. Heat Mass Trans. 55 (2012) 7812-7822.

[20] D. Iyi, D. R. Hasan, Natural Convection Flow and Heat Transfer in an Enclosure Containing Staggered Arrangement of Blockages, Proc. Eng. 105 (2015)176- 183.

[21] J. Ma, F. Xu, Unsteady natural convection and heat transfer in a differentially heated cavity with a fin for high Rayleigh numbers, Appl. Therm. Eng. (99) (2016) 625-634.

[22] M. Ghalambaz, E. Jamesahar, M. A. Ismael, Fluid-structure interaction study of natural convection heat transfer over a flexible oscillating fin in a square cavity, Int. J. Heat Mass Trans. 111 (2017) 256–273.

[23] A. Azimifar, S. Payan, Optimization of characteristics of an array of thin fins using PSO algorithm in confined cavities heated from a side with free convection, Appl. Therm. Eng. 110 (2017) 1371- 1388.

[24] H. T. Chen, M. Lin, J. R Chang, Numerical and experimental studies of natural convection in a heated cavity with a horizontal fin on a hot side wall, Int. J. Heat Mass Trans. 124 (2018) 1217–1229.

[25] A. I. Alsaberya, M. A. Sheremet, M. Ghalambaz, M. J. Chamkha, H. Hashim, Fluid-structure interaction in natural convection heat transfer in an oblique cavity with a flexible oscillating fin and partial heating, Appl. Therm. Eng. 145 (2018) 80–97.

[26] S. Pandey, Y. G. Park, M. Y. Ha, An exhaustive review of studies on natural convection in enclosures with and without internal bodies of various shapes, Int. J. Heat Mass Trans. 138 (2019) 762-795.

[27] Y. Zhou, L. Zhang, S. Bu, C. Sun, W. Xu, Y. Xiao, L. Liu, Study on Heat Transfer Characteristics of the Whole Plate Fin Tube Cooler, Int. J. Thermofluid Science and Technology 7 (2020) 1- 16.

[28] M. Fayz-Al-Asad1, M. J. H. Munshi, M. Manirul Alam Sarker, Effect of Fin Length and Location on Natural Convection Heat Transfer in a Wavy Cavity, Int. J. Thermofluid Science and Technology 7 (2020) 18- 30.

[29] M. Eslami, F. Khosravi, H.R. Fallah Kohan, Effects of fin parameters on performance of latent heat thermal energy storage systems: A comprehensive review, Sust. Energy Techn. Asses. 47 (2021) 101449

[30] S. H. Patankar, Numerical heat transfer and fluid flow, Hemisphere Publishing Corporation, New York, USA, 1980.

[31] M. T. Manzari, An explicit finite element algorithm for convective heat transfer problems, Int. J. Numer. Meth. Heat Fluid Flow 9 (1999) 860-877.

[32] D. A. Mayne, A. S. Usmani, M. Crapper, h-Adaptive finite element solution of high rayleigh number thermally driven cavity problem, Int. J. Numer. Meth. Heat Fluid Flow 10 (2000) 598- 615.

[33] F. Corvaro, M. Paroncini, An experimental study of natural convection in a differentially heated cavity through a 2D-PIV system, Int. J. Heat Mass Trans. 52 (2009) 355–365.